
Expected hypervolume improvement for simultaneous multi-objective and multi-fidelity optimization

Faran Irshad

Faculty of Physics

LMU Munich

Am Coulombwall 1

85748 Garching, Germany

faran.irshad@lmu.de

Stefan Karsch

Faculty of Physics

LMU Munich

Am Coulombwall 1

85748 Garching, Germany

stefan.karsch@lmu.de

Andreas Döpp

Faculty of Physics

LMU Munich

Am Coulombwall 1

85748 Garching, Germany

a.doepf@lmu.de

Abstract

Bayesian optimization has proven to be an efficient method to optimize expensive-to-evaluate systems. However, depending on the cost of single observations, multi-dimensional optimizations of one or more objectives may still be prohibitively expensive. Multi-fidelity optimization remedies this issue by including multiple, cheaper information sources such as low-resolution approximations in numerical simulations. Acquisition functions for multi-fidelity optimization are typically based on exploration-heavy algorithms that are difficult to combine with optimization towards multiple objectives.

Here we show that the expected hypervolume improvement policy can act in many situations as a suitable substitute. We incorporate the evaluation cost either via a two-step evaluation or within a single acquisition function with an additional fidelity-related objective. This permits simultaneous multi-objective and multi-fidelity optimization, which allows to accurately establish the Pareto set and front at fractional cost. Benchmarks show a cost reduction of an order of magnitude or more. Our method thus allows for Pareto optimization of extremely expansive black-box functions.

The presented methods are simple and straightforward to implement in existing, optimized Bayesian optimization frameworks and can immediately be extended to batch optimization. The techniques can also be used to combine different continuous and/or discrete fidelity dimensions, which makes them particularly relevant for simulation problems in plasma physics, fluid dynamics and many other branches of scientific computing.

Introduction

Optimization of black-box functions is a very common task across numerous disciplines such as computer science, engineering and physics (Theodoridis 2015; Arora 2019). While these problems are well understood for some kinds of functions, there exist various properties that can make black-box functions very difficult to optimize towards a certain goal. First of all, optimization becomes increasingly challenging the more input dimensions the function has. This situation is well known as the *curse of dimensionality* and, as a result, optimization becomes particularly challenging if single evaluations of the problem are very expensive or slow.

The situation becomes even more complicated when the optimization goal, the *objective*, is not straightforward to define but represents a combination of desirable outcomes. Examples for this situation are plentiful and range from everyday cost-benefit problems to science cases such as the one that motivated this study, namely the optimization of multiple beam parameters (charge, energy,

etc.) in a particle accelerator (Shalloo et al. 2020; Jalas et al. 2021). In most of these scenarios optimization is performed by combining the 'vector' of individual outcomes into a single 'scalar' metric. This can for instance be done by weighed addition/multiplication of the individual objectives or by constraining individual objectives (Paria, Kandasamy, and Póczos 2020; Deb 2014). It is however a major problem of such single-objective optimizations that the weights or constraints set during scalarization are entirely empirical and may not reflect the best possible outcome for the desired goal. Furthermore, in many cases individual objectives may be conflicting in nature, be it the aforementioned cost-benefit scenario or due to fundamental properties such as energy conservation in a charge versus energy optimization. In this case, one needs to find a trade-off that optimally balances the individual objectives. This is difficult to achieve with scalarized objectives because the possible outcomes are not known prior to observation and a combined objective is always biased towards one particular trade-off of the underlying, conflicting objectives. Consequently one needs to execute the optimization multiple times with different settings to find the most suitable way to combine multiple objectives of the desired application, which accordingly makes the entire optimization much more expensive.

A more versatile strategy is to directly explore the trade-off between different objectives and *then* choose the optimal combination of objectives to reach the desired outcome. A useful concept describing this situation of not just a single optimum but a set of optimal points in the multi-dimensional objective space is the *Pareto efficiency*, which is visualized as the *Pareto front* (Branke et al. 2008). To describe the Pareto front the notion of *domination* is outlined with two objective functions ($f_1(x), f_2(x)$). A point in this 2D output space $p_1 = (y_1, y_2)$ is said to be *dominated* if there exists another point $p'_1 = (y'_1, y'_2)$ that has equal values for all objectives and a higher value for at least one $y'_1 > y_1 \wedge y'_2 \geq y_2$. The Pareto front then consists of all the *nondominated* points. An example of a Pareto front is shown in black in Figure 1. A metric for the quality of a Pareto front is known as the hypervolume (Zitzler and Thiele 1999) that captures the n-dimensional volume covered by the Pareto front from a reference point. In the case of two objectives, which is easier to visualize and thus used frequently in this manuscript, the hypervolume is easily visualized as the area between the Pareto front and the reference. This reference point is usually chosen by the user to lie below the observable objective function values. An increase in the hypervolume then indicates domination of points in the current Pareto front by an observed point. The points in the input space points that yield the Pareto front are known as the *Pareto set*. It is important to note that some points within the Pareto set may be connected along a continuous path, but this is not necessarily the case for the entire Pareto set, in particular in presence of local optima (cf. left part of Fig.1).

Multi-objective optimization is relevant for many optimization problems and evolutionary algorithms have proven particularly efficient for this purpose (see e.g. Deb and Sundar 2006). More recently, methods based on Gaussian process regression have started to be explored for multi-objective optimization of black box functions that are very expensive to evaluate (Knowles 2006; Ponweiser et al. 2008; M. Emmerich and J.-W. Klinkenberg 2008). An early example of optimization strategies falling into this category is Kriging (Krige 1951), which was developed in the context of oil field exploration (Matheron 1963). Recently often referred to as Bayesian optimization (Shahriari et al. 2015), this technique builds a surrogate model of the objective field based on existing measurements using Gaussian process (GP) regression and then uses fast optimizers to suggests the next location to probe the system. However, the adoption of multi-objective Bayesian optimization in the context of costly black box functions remains constraint by the total computational cost of an optimization run.

In this article we discuss how an existing Bayesian optimization policy, namely expected hypervolume improvement, can be extended to allow simultaneous multi-objective and multi-fidelity optimization. The method makes efficient use of cheaper approximations of the black box function, each of different fidelity, to establish the Pareto front for lower total cost. The manuscript is structured as follows: After an introduction to Bayesian optimization via Gaussian process regression (1.1), we discuss common acquisition functions used for single-objective, single-fidelity optimization (1.2). We then outline how these policies are generalized to either multi-fidelity (1.3) and multi-objective (1.4) optimization. In Section 2 we then use these concepts to devise policies to perform combined multi-fidelity, multi-objective optimization in either two steps (2.1) or in a combined, single step (2.2). We benchmark our results for different test functions, showing significantly faster convergence towards the Pareto front than for Bayesian optimization without multiple fidelities (2.3). In Section 3 we summarize our results and give an outlook on potential applications.

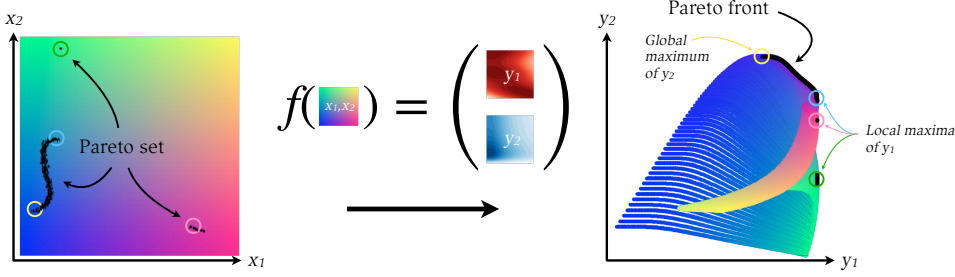


Figure 1: **Pareto front.** Illustration how a multi-objective function $f(\mathbf{x}) = \mathbf{y}$ acts on a two-dimensional input space $\mathbf{x} = (x_1, x_2)$ and transforms it to the objective space $\mathbf{y} = (y_1, y_2)$ on the right. The entirety of possible input positions is uniquely color-coded on the left and the resulting position in the objective space is shown in the same color on the right. The Pareto front is the ensemble of points that dominate others, i.e. that give the highest combination of y_1 and y_2 . The corresponding set of coordinates in the input space is called the Pareto set. Note that both Pareto front and Pareto set may be continuously defined locally, but can also contain discontinuities when local maxima get involved. In this example, f is a modified version of the Branin-Currin function from (Dixon 1978; Currin et al. 1991) that exhibits a single, global maximum in y_2 but multiple local maxima in y_1 , see also illustration in the center.

1 Bayesian approaches for multi-fidelity or multi-objective optimization

1.1 Bayesian optimization via Gaussian process regression

Gaussian processes (GP) are a distribution over functions of random variables in a continuous domain and serve as a model for the black-box objective function (Rasmussen 2003). The GP can be completely described by a mean and a co-variance or kernel function. The mean function describes the average value of the objective function in the parameter space while the kernel captures the relation between two different points in the parameter space. Prior information of the black-box function $f(\mathbf{x})$ can be encoded either in the mean function or in the kernel. By convention at the start of the optimization the mean is taken to be zero everywhere whereas the prior information about $f(\mathbf{x})$ is encoded in the kernel. Once the black-box function is evaluated at a certain number of positions x_i , the GP is updated conditioned on the evaluated values y_i . This so-called "posterior" distribution $g(\mathbf{x})$ is, in contrast to $f(\mathbf{x})$, inexpensive to probe. After obtaining the model, the task of finding the next evaluation point is performed by the acquisition function that uses the inexpensive posterior distribution $g(\mathbf{x})$. In essence, the problem of optimizing the expensive black-box function is reduced to one of optimizing an inexpensive acquisition function for which many efficient algorithms exist.

Acquisition functions are a broad class of functions that can be constructed using the GP model mean and variance. The quality of an acquisition function can be judged by its ability to reach the global optimum in as few evaluations of the objective function as possible. This can be best explained through a series of diagrams shown in Figure 2, where runs of a Bayesian optimization are shown starting from three initial points. After a GP model is constructed giving a mean (solid blue line) and a variance (shaded region), the acquisition function is constructed (bottom plot). This acquisition function is then optimized using e.g. gradient methods to find its maximum, which is the point where the next evaluation of the black-box objective function will be taken. The choice of the acquisition function thus has significant impact on the convergence of the Bayesian optimization to the global optimum and the next section summarizes some of the most popular policies described in the literature.

1.2 Single-objective, single-fidelity optimization

In this section we will briefly review some of the most common acquisition functions used for the optimization of a single objective from a single information source. We assume that the objective function has been evaluated n times yielding input-output pairs $[x_n, y_n]$ over which a posterior mean $\mu_n(x)$ has been calculated. All of the acquisition functions suggest the next

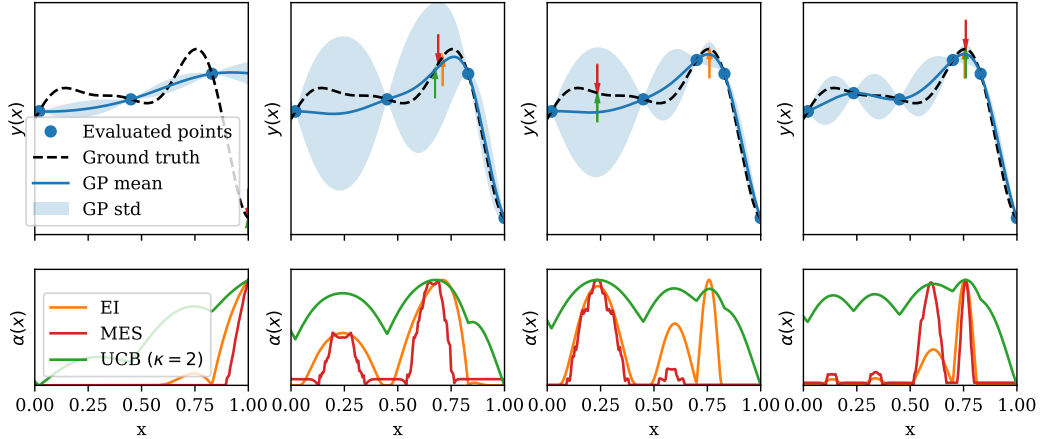


Figure 2: **Consecutive iterations of Bayesian maximization of the Forrester test function.** *Top:* The dashed black line represents the true function that is being optimized. The blue line is the GP regression mean with a shaded region around it representing the standard deviation. The blue dots are the points that were evaluated. Arrows indicate the next measurement point suggested by the respective acquisition functions from the bottom plot, showing the different prioritization towards exploration and exploitation. *Bottom:* Evaluations of three different metrics, i.e. expected improvement (EI, Eq. 1), max-value entropy search (MES, cf. Eq.4) and upper confidence bound (UCB, Eq. 5 with $\kappa = 2$) for each step in the upper plot.

point by maximizing a quantity generated using the evaluated points and the posterior distribution $x_{n+1} = \arg \max_{x \in \mathcal{X}} D^n(x)$ where D^n is one of the acquisition function described below.

The arguably most common acquisition function in Bayesian optimization is known as Expected Improvement (EI) (Mockus 1994). It proposes the next point to be probed based on the expected improvement over the current optimal objective value y^* . We can write the acquisition function as

$$EI_n = \mathbf{E}[\max(f_{n+1}(x) - y^*, 0)], \quad (1)$$

where $f_{n+1}(x)$ is calculated using the GP posterior to compute EI. A variation of EI is the knowledge gradient (KG) acquisition function (P. I. Frazier, W. B. Powell, and Dayanik 2008; Scott, P. Frazier, and W. Powell 2011). In KG we essentially 'trust' the posterior model and select our next point in the Bayesian optimization not conditioned on the best observable, but the best value of the posterior mean. The KG acquisition function is

$$KG_n = \mathbf{E}[\max_{x \in \mathcal{X}}(\mu_{n+1}(x)) - \max_{x \in \mathcal{X}}(\mu_n(x))], \quad (2)$$

which is more exploratory than EI because it is influenced by how the posterior changes over the whole domain. This makes it attractive for incorporating multiple fidelities.

Another class of acquisition functions are known as information-theoretic where the purpose is to utilize the mutual information between the maximizing location x^* and observed data set (Hennig and Schuler 2012). Entropy search (ES) is the first of these and is mathematically represented as

$$ES_n = I([x_{n+1}, y_{n+1}]; x^* | [x_n, y_n]) = H(p_n(x^*)) - \mathbf{E}[H(p_n(x^* | [x_{n+1}, y_{n+1}]))], \quad (3)$$

where H denotes the Shannon's entropy. The left term above depicts the entropy of the posterior of the maximizing location x^* while the right term depicts an expectation over the entropy after an additional sample. In higher input dimensions it becomes difficult to evaluate the mutual information between the point to be queried and the maximizing location x^* . Another cheaper to evaluate entropy-based acquisition function known as Max-value entropy search (MES) (Wang and Jegelka 2017) utilizes the mutual information I between the maximum value y^* instead of x^* .

$$\begin{aligned} MES_n &= I([x_{n+1}, y_{n+1}]; y^* | [x_n, y_n]) \\ &= H(p_n(y^* | [x_n, y_n], x_{n+1})) - \mathbf{E}[H(p_n(y | [x_n, y_n], x_{n+1}, y^*))] \end{aligned} \quad (4)$$

This is computationally cheaper than ES to evaluate while maintaining comparable or better performance.

For completeness, the upper confidence bound policy (UCB), or lower confidence bound (Cox and John 1992) for minimization tasks, is

$$\text{UCB}(x) = \mu(x) - \kappa\sigma(x) \quad (5)$$

where κ is a parameter to trade off exploration versus exploitation. UCB is a much more simpler acquisition function that works well in practice and can also be extended to multi-fidelity applications easily.

1.3 Single-objective, multi-fidelity optimization

Many single-objective policies can be extended to include multiple information sources (Huang et al. 2006; Picheny et al. 2013; Swersky, Snoek, and Adams 2013; Klein et al. 2017; McLeod, Osborne, and Roberts 2017; Zhang et al. 2017). This is essentially done by adding new dimensions to the input space of the problem that describes the accuracy or *fidelity* of the data. Typically, low fidelity information sources are cheaper to probe than high fidelity sources, which means there is a trade-off between data fidelity and cost.

Denoting the search parameters as \mathbf{x} and fidelity parameters as \mathbf{s} , we can build a surrogate model that incorporates information from $\mathbf{f}(\mathbf{x}, \mathbf{s})$. The main difference to the single-objective scenario is that we are ultimately most interested in the best value at the target fidelity, which in most use cases corresponds to the most expensive, highest fidelity sources. It should be noted that if we were to treat the fidelity dimensions like other input dimensions, the optimizer may find the optimal numerical value lies at a low fidelity and might not explore the high-fidelity dimension. On the other hand, if the high-fidelity dimension typically yields higher values in general, the acquisition function of a maximization problem might not incorporate many measurements from lower fidelities. Multi-fidelity optimization algorithms therefore need to effectively leverage information versus cost.

An intuitive solution to this problem is the two-step approach by Lam, Allaire, and Willcox 2015. Here the selection of the next point to probe in \mathbf{x} is done separately from the fidelity choice \mathbf{s} . Regarding the first, Lam et al. use an EI policy that is conditioned and evaluated at the target fidelity only. It also incorporates measurements at different fidelity by projecting them to the target fidelity using the surrogate model. Once a suitable position has been identified in \mathbf{x} , the ideal fidelity for probing this point is chosen by rating the predicted reduction in uncertainty or gain in knowledge with the computational cost involved.

Both selection of the next point and weighting by the expected knowledge gain per unit cost can also be combined in a single step. However, due to the aforementioned problems, it is usually necessary to use more exploratory algorithms for this purpose. In particular MES and KG acquisition functions are adapted with minor changes for multi-fidelity optimization. For KG, instead of being conditioned on the best value of the posterior mean, they are conditioned on the best value of the posterior mean at the target fidelity $s^* \max_{x \in \mathcal{X}} (\mathbf{f}(\mathbf{x}, s^*))$. In the case of MES the mutual information between the maximum value y^* at the highest fidelity with the data set is maximized. This gain of information is then divided by the computational cost that is a function of fidelity (Takeno et al. 2020). We can write the acquisition function of this multi-fidelity MES as

$$\text{MF-MES}_n = \frac{H(p_n(y^* | [x_n, y_n], x_{n+1})) - \mathbf{E}[H(p_n(y | [x_n, y_n], x_{n+1}, y^*))]}{\text{cost}(s)}. \quad (6)$$

Similar multi-fidelity policies exist for other exploratory acquisition functions such as the Upper Confidence Bound (Kandasamy, Dasarathy, Poczos, et al. 2016; Kandasamy, Dasarathy, Schneider, et al. 2017) or Knowledge gradient (Wu and P. I. Frazier 2018; Wu, Toscano-Palmerin, et al. 2020).

1.4 Multi-objective, single-fidelity optimization

As we outlined in the introduction, it is desirable in many cases to optimize not only towards a single, scalarized objective, but to establish a combination of solutions that maximizes different objectives. In this case the function that is being maximized can be expressed as a vector of functions

$$\mathbf{f}(\mathbf{x}) = \begin{pmatrix} f_1(\mathbf{x}) \\ f_2(\mathbf{x}) \\ \dots \end{pmatrix}$$

that are evaluated to yield output vectors

$$\mathbf{y}(\mathbf{x}) = \begin{pmatrix} y_1(\mathbf{x}) \\ y_2(\mathbf{x}) \\ \dots \end{pmatrix}$$

As mentioned in the introduction, a useful criteria employed in such a Multi-objective Bayesian optimization is known as the Hypervolume Indicator. Hypervolume (HV) is defined as the n-dimensional volume of the output subspace covered from a reference point, always taken to be zero in this work, to a set of points known as the Pareto front (\mathcal{P}). This Pareto front as depicted in Fig.1 is the set of points that dominate all other points in the space. Using this definition of HV, we can then proceed to define Hypervolume Improvement (HVI) as

$$\text{HVI}(\mathcal{P}, y) = \text{HV}(\mathcal{P} \cup y) - \text{HV}(\mathcal{P}) \quad (7)$$

Equation 7 describes essentially the difference between the current hypervolume and one with an additional output point y (Yang, M. Emmerich, A. Deutz, and Bäck 2019). If the set of points making up \mathcal{P} already dominate y then $\text{HVI} = 0$, because there is no hypervolume gained by adding the point y .

HVI can be used to generalize the expected improvement policy described in section 1.2 to the multi-objective scenario. First proposed by M. T. Emmerich, Giannakoglou, and Naujoks 2006, this method is called *Expected Hypervolume Improvement (EHVI)*. Following the definition from Yang, M. Emmerich, A. Deutz, and Bäck 2019, we can write this as

$$\text{EHVI}(\mu, \sigma, \mathcal{P}, y) = E[\text{HVI}] = \int \text{HVI}(\mathcal{P}, y) \cdot \text{PDF}_{\mu, \sigma}(y) dy, \quad (8)$$

where the probability density function $\text{PDF}_{\mu, \sigma}$ is the independent multivariate normal distribution with mean μ and standard deviation σ . This infill criterion has been demonstrated to achieve a good convergence to the true Pareto front (Cockuyt, Deschrijver, and Dhaene 2014; Luo, Shimoyama, and Obayashi 2014; Shimoyama, Jeong, and Obayashi 2013).

One of the usual criticism of EHVI has been of the time complexity involved in calculating it. A first closed form calculation of EHVI was implemented by M. T. Emmerich, A. H. Deutz, and J. W. Klinkenberg 2011 with a computational complexity $\mathcal{O}(n^3 \log n)$ for a 2-D case. Over the years with efforts by Hupkens et al. 2015, M. Emmerich, Yang, et al. 2016 and Yang, M. Emmerich, A. Deutz, and Fonseca 2017 the time complexity for 2-D and 3-D case has been reduced to $\mathcal{O}(n \log n)$. In this work an implementation of EHVI available on BoTorch based on estimating gradients using auto-differentiation is used as described by Daulton, Balandat, and Bakshy 2020. This exploits the high number of cores that are available with modern GPUs to make EHVI optimization fast and applicable to real-world scenarios. Since the simulations discussed in this work are assumed to be much more expensive, the overhead from EHVI optimization is insignificant.

2 Bayesian multi-objective and multi-fidelity optimization

Due to their exploratory nature, multi-fidelity algorithms that act on a scalar objective can in principle also find a Pareto front. However, due to the necessary scalarization step, these functions are always biased towards a certain part of the Pareto front. A more efficient, holistic approach is to take both multi-objective and multi-fidelity information into account. A first paper reporting such an approach for discrete fidelity levels was recently published by Belakaria, Deshwal, and Doppa 2020. Being mostly motivated by applications in neural network training, the approach from this paper is however limited to scenarios where higher fidelities yield higher objective values. The assumption of objective values at lower fidelities being upper bounded by the values at highest fidelity in general does not hold true for many use cases such as numerical simulations of physical systems. To remedy this issue we present two new approaches for Bayesian multi-objective and multi-fidelity optimization using either two evaluation steps for objectives and fidelity, respectively or combining both into a single prediction.

Many studies motivated by applications such as neural network training use an exponential decay kernel by default. In this paper, we have k number of GP_1, GP_2, \dots, GP_k models modelling k objective functions $f_1, f_2, \dots, f_k(\mathbf{x})$. Each of these functions also has an input fidelity parameter s that implies greater accuracy with higher values. In this case highest fidelity evaluation of these

objectives functions do not necessarily yield highest objective values. The fidelity parameter is also modelled by the GP outlined above with a Matern 5/2 kernel representing a problem of the nature $d + 1 \rightarrow k$ where d is the input dimension, k is the output dimension (number of objective functions) and $+1$ represents the fidelity dimension. The use of the Matern 5/2 kernel permits us to model a more general form of fidelity dependence, in contrast the strictly monotonically increasing dependence assumed in (Belakaria, Deshwal, and Doppa 2020). Our benchmark functions (see Sec.2.3) are thus also design for not having the highest objective values for the highest fidelity as discussed before. There the points on the Pareto front at the highest fidelity do not completely dominate the points on the Pareto front at any lower fidelity. Hence the algorithm will aim to reproduce the Pareto front at the highest fidelity rather than achieving the highest possible Pareto front.

2.1 Two-step optimization

Analogous to the work by Lam, Allaire, and Willcox 2015, we can use MO restricted to a single target fidelity to select the next position x_{n+1} to probe and then the fidelity s_{n+1} that provides highest information gain per unit cost at x_{n+1} is selected .

Here we are going to use EHVI to suggest the next point in the input space x_{n+1} and combine it with the MF-MES method that maximizes information gain on a scalarized objective giving the fidelity point s_{n+1} . The scalarization is done by summing all the objectives with equal weights. In this process we call 2-step multi-objective multi-fidelity (2-step MOMF), the selection of the input domain x is disjointed from the selection of the fidelity point s . Here, we can also utilize any other multi-fidelity acquisition function such as KG or UCB discussed before for selecting the fidelity parameter s . The working of the 2-step MOMF is outlined in algorithm 1.

For a single fidelity dimension, the multi-fidelity step takes a negligible amount of time and the method can be extended to multiple fidelity dimensions. Similar to Lam et al., our two-step multi-fidelity implementation is not simultaneously optimizing the different objectives and fidelities.

Algorithm 1 Two-Step Multi-Objective Multi-Fidelity Optimization (2-step MOMF)

2.2 Single-step optimization

As discussed earlier, single-step multi-fidelity optimization with greedy, myopic algorithms is difficult because the optimal numerical value may lie outside of the target fidelity plane, in which case the optimizer has no incentive to probe this fidelity. However, in case of multi-objective optimizers we can alleviate this issue by introducing an additional, fidelity-related objective. To illustrate this approach, we use a simple one-dimensional problem with an additional fidelity dimension, based on Forrester's function. In this case, the output of the function is a vector of the form

$$f(x, s) = \begin{pmatrix} f_1(x, s) \\ f_2(s) \end{pmatrix}$$

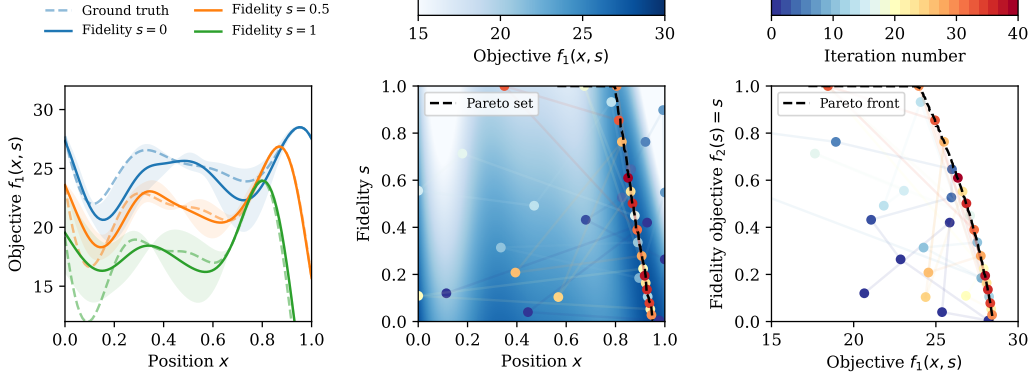


Figure 3: **Multi-fidelity optimization via hypervolume improvement** of a modified Forrester function. *Left*: Mean and variance (shaded curve) of the fitted Gaussian process after 40 iterations of the optimizer. The true values are indicated as dashed lines. *Center*: Map of the objective values $f_1(x, s)$ and sampled points colored according to the iteration number. This illustrates how the optimizer first explores at low fidelity and then moves along the Pareto set. *Right*: Same optimization in the objective space, showing how the optimizer tries to increase the hypervolume, which is simply the area in 2D, below the Pareto front.

The fidelity objective function should be monotonically increasing and may be chosen as simple as $f_2(s) = s$. In this case, the multi-fidelity expected hypervolume optimization (MF-EHVI) is simultaneously trying to optimize the function objective and the fidelity objective. Because of the increasing fidelity objective, the optimizer will always explore the target fidelity level and try to increase the hypervolume enclosed within the Pareto front of $f_1(x, s)$ and $f_2(s)$. As in any multi-fidelity scenario with difference in cost, we can use a cost-related penalizer such that the acquisition function will always probe the point with the largest ratio between the expected hypervolume improvement and the associated cost. In summary, the acquisition function will optimize the knowledge about the Pareto front and Pareto set per unit cost.

Figure 3 shows an example how this multi-fidelity version of the EHVI acquisition function, henceforth called single-step multi-objective multi-fidelity (1-step MOMF), optimizes the 1D Forrester function by incorporating information from lower fidelity data with reduced cost. The cost in this test case is modeled as $C(s) = \exp[a \cdot s]$, with $a = 5$ such that the cost for an evaluation at maximal fidelity is about 150 times higher than at low fidelity. The main assumption of 1-step MOMF is that the Pareto set underlying the Pareto front belongs to a similar region of the search space so that the information is efficiently translated between fidelities. It should be noted that this method, as all multi-fidelity approaches that transfer knowledge, is less efficient if the Pareto set moves significantly between fidelities.

While our example uses a very simple fidelity objective, $f_2(s) = s$, the behavior of the optimizer can be further tuned via the fidelity objective function $f_2(s)$ and can take into account prior knowledge about the information gain from different fidelities. For instance, if fidelity corresponds to the resolution of a numerical simulation it is in many cases expected that the result eventually converges with little extra information at increasing cost. This type of behavior can be accounted for via the fidelity objective, e.g. by using an objective with decreasing return such as $f_2(s) = \tanh(s)$. It is also conceivable to take behavior such as numerical convergence dynamically into account during optimization.

Last, we would like to mention that we can also extend the method to include multiple fidelity dimensions s^m where m is the number of fidelity dimensions, which is useful for multi-dimensional numerical models with individual resolution parameters. Depending on the problem, these individual fidelity dimensions may still be treated via a single, combined fidelity objective or as individual dimensions of the optimization problem. It should be noted, however, that the EHVI algorithm does not scale very effectively to many dimensions and the 2-step MOMF may be preferable if many fidelity dimensions are to be optimized individually.

Algorithm 2 Single-Step Multi-Objective Multi-Fidelity Optimization (1-step MOMF)

2.3 Comparison and benchmark

In this section we will describe the results of our proposed single-step and two-step MOMF algorithms. As discussed above, the algorithm on entropy-search methods (for 2-step MOMF) and expected hypervolume improvement acquisition functions (for both 1-step and 2-step MOMF). All bench-marking is performed by modifying existing implementations of MES and EHVI in the BoTorch package (Balandat et al. 2020) to the multi-objective, multi-fidelity problem.

To assess the performance of the methods, we use multi-fidelity modifications of the popular Branin-Currin (2-D) and Park (4-D) test functions. The function definitions are given in the Appendix. The cost function for the different fidelities is modeled as an exponential function of the form $C(s) = \exp(4.8 \cdot s)$ resulting in a ratio of about 120:1 between the highest ($s = 1$) and lowest ($s = 0$) fidelity. This cost function represents a realistic model for a scenario such as computational physics simulations, which can easily take from 10 minutes to 20 hours to run, depending on parameters such as the numerical resolution, number of spatial dimensions and so forth.

Both MOMF algorithms are initialized with five starting points that are randomly distributed in the input search space. The single-fidelity EHVI optimizer is initialized with a single point at the highest fidelity $s = 1$ and thus starts at an initial cost of $C(1) \simeq 120$. Meanwhile, the fidelity of initial points for the MOMF optimizers is drawn from a cost-aware probability distribution of the form $p(s) \propto 1/C(x)$, resulting on average in a five-times lower initialization cost. As the choice of initial points can influence the performance of the optimization, we run each optimizer 10 times with different initialization to attain more robust statistics on the convergence of the algorithms. For hypervolume calculation, the points taken during the optimization run are used as training inputs for a GP model while a random input sample of 10000 points at the highest fidelity are taken as test inputs. From these 10000 points a set of non-dominated points and consequently the hypervolume is calculated at each iteration step. Please note that the estimated hypervolume may occasionally decrease between iterations (see for instance 2-step MOMF at cost ~ 600 in Fig.4). This is because we calculate the hypervolume via the GP and not only via the dominating measurements at maximum fidelity. When a point is added to the training inputs, this can have the effect of decreasing the hypervolume temporarily since the model might predict differently at other places of the 2-D space. After subsequent learning of the objective function this effect is minimized since the GP model becomes more certain of its predictions. Furthermore, in the first two iterations due to lack of training points for the GP model we obtain a large set of non-dominated points making this calculation computationally expensive, thus without any loss of information this calculation is after four iterations. This is the reason the hypervolume points for the EHVI in the following figures start at a cost of 480. Last, the number of iterations for the MOMF algorithms was fixed to 120 while the EHVI ran for 80 iterations. For the EHVI the total cost was 9600 while the MOMF algorithms stopped at variable costs ranging from 1500 to 4000.

In Figure 4 an optimization of the multi-fidelity versions of Branin and Currin (Dixon 1978; Currin et al. 1991) functions is shown. A single representative trial that was close to the mean hypervolume as a function of cost is depicted on the top left. The regular steps along the cost axis for EHVI indicate a fixed cost at the highest fidelity, while for both the MOMF it can be seen that step sizes are irregular. The MOMF algorithms take a few points at intermediate fidelities before taking a

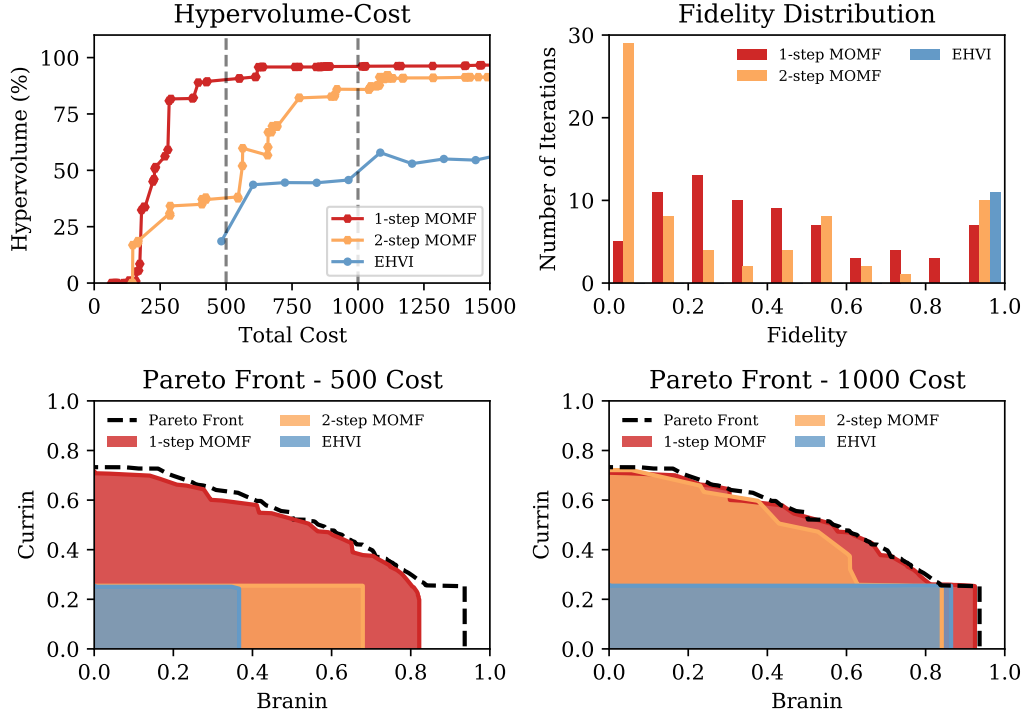


Figure 4: **Benchmark with 2-D-Branin-Currin problem.** *Top Left:* Hypervolume of a single representative trial expressed as a percentage of the total hypervolume versus total cost for both MOMF versions and single-fidelity EHVI. *Top Right:* The number of points taken at different fidelities for the representative trials shown on the left. The 1-step MOMF takes more iterations at intermediate fidelities when compared with 2-step MOMF which has relatively high peaks at fidelity 0 and 1. Note that the EHVI only takes points at the highest fidelity. *Bottom Left:* The Pareto front for each of the three algorithms for the same trial at a cost of 500 (indicated by dashed line in the figure on the top left). The dashed black line represents the true Pareto front calculated from 10000 random points. The area represents the amount of Pareto front covered by each algorithm. The 1-step MOMF has already found values in the trade-off region and close to the individual maxima of the Branin and Currin functions. The 2-step MOMF is approaching the maximum of the Branin function but both 2-step MOMF and EHVI have yet to explore the trade-off points. *Bottom Right:* The Pareto front for a cost of 1000 cost for a single representative trial, clearly showing how the 1-step MOMF has reached an accurate representation of the Pareto front while the conventional, single-fidelity EHVI algorithm has only discovered a small fraction of the Pareto front.

high fidelity point. This can also be seen in top right of the figure where the distribution of selected fidelities is shown for each algorithm. Interestingly, we observe a different behavior between the two MOMF algorithms. The 2-step MOMF takes considerably more points at the lowest fidelity, while the 1-step MOMF takes much more intermediate fidelity points, possible because of the joint optimization of both input and fidelity space.

The bottom part of Figure 4 depicts the behaviour of the Pareto front at two different costs. The black-dashed line represents the true Pareto front calculated using 50000 random points. Here it can be seen that the 1-step MOMF already has a good coverage of the trade-off region and the maximum of the Currin function. The EHVI and 2-step MOMF at a cost of 500 have much less hypervolume coverage. At a cost of 1000 the EHVI has optimized the Branin function but still has not explored the trade-off region. The 2-step MOMF at a cost of 1000 is in a similar state as that of 1-step MOMF at a cost of 500. Meanwhile, the 1-step MOMF has reached near 100% hypervolume coverage.

For the estimation of the cost advantage we use the average hypervolume cost curves from ten runs (shown at the left in Figure 6). Taking 90% convergence as a threshold, there is an order

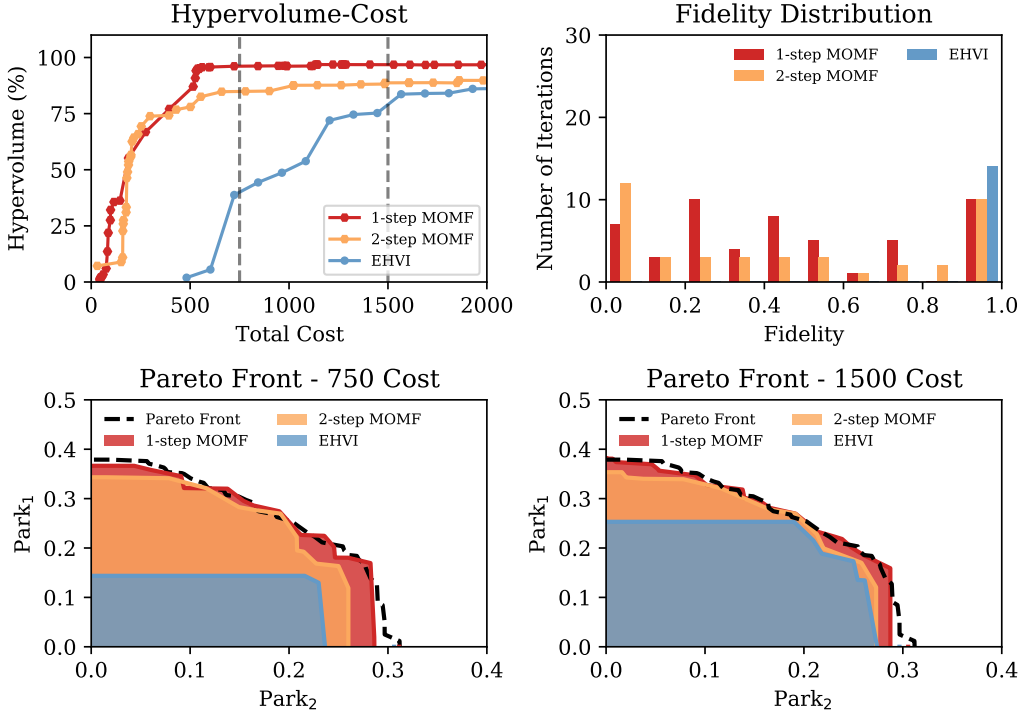


Figure 5: **Benchmark with 4-D-Park_{1,2} problem.** *Top Left:* Hypervolume of a single representative trial expressed as a percentage of the total hypervolume versus total cost for both MOMF versions and single-fidelity EHVI. *Top Right:* The number of points taken at different fidelities for the representative trials shown on the left. The 1-step MOMF in this case has a higher number of points taken at the highest fidelity. This is because once it has converged it takes 6 points at the highest fidelity to increase hypervolume. The 2-step MOMF as seen in Branin-Currin case takes less intermediate fidelity points when compared to the 1-step MOMF. *Bottom Left:* The Pareto front for each of the three algorithms for the same trial at a cost of 750 (indicated by dashed line in the figure on the top left). The area represents the amount of Pareto front covered by each algorithm. The 1-step MOMF has already converged to almost 95% of the total hypervolume. The 2-step MOMF also converged but to a lower overall hypervolume. The EHVI at this cost has only found maximum of Park 2 function. *Bottom Right:* The Pareto front for a cost of 1500 cost showing little changes in both MOMF Pareto fronts, but a better coverage for the EHVI. At this cost the EHVI still has not reached the hypervolume that the 1-step MOMF reached at a cost of 750.

of magnitude cost advantage for the 1-step MOMF over the EHVI. The EHVI converged to 90% at about a cost of 9600 while the 1-step MOMF reached the same hypervolume at a cost of 730, resulting in a cost reduction factor of ~ 13 . Moreover the 1-step MOMF converged to a higher hypervolume percentage (97%) when compared with final convergence of 90% for EHVI.

Figure 5 depicts a representative trial run results of the same three algorithms for the optimization run of modified Park functions (Park 1991). The top left sub-figure shows the hypervolume percentage covered versus total cost for the MOMF and EHVI runs. The Park problem shows a similar behavior regarding the fidelity distribution, i.e. the 2-step MOMF concentrates on points at minimum ($s = 0$) and maximum ($s = 1$) fidelity, while the 1-step MOMF takes more intermediate fidelity points. On the bottom two plots of Figure 5 we see the evolution of the Pareto fronts for the 3 optimizers. The 1-step MOMF already at a cost of 500 has converged to a hypervolume coverage of 94%, hence its Pareto front at a cost of 750 is close to the true Pareto front. The 2-step MOMF also has started exploring the trade-off region and consequently pushes out the Pareto front slightly up to a cost of 1500, as shown on the right. The EHVI at the cost of 750 has found points close to Park 2 maximum and thus explores the trade-off region at a cost of 1500. The cost advantage estimation is again done using the mean hypervolume versus total cost curves generated using 10 trials as shown in Figure 6.

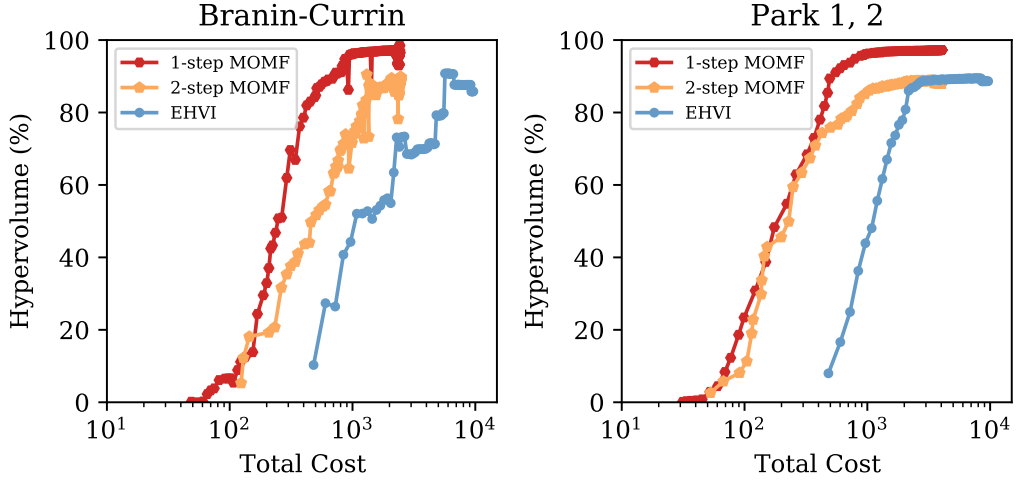


Figure 6: **Mean Hypervolume of 10 trials for Branin-Currin and Park functions.** *Left:* Mean Hypervolume as a percentage of the total for 10 trials of Branin-Currin optimization is illustrated. The total cost is in the log scale to depict the large differences in the cost. The dips seen in the curve around 900 are due to the method of calculating the hypervolume described earlier. When considering convergence to 90% hypervolume an order of magnitude cost difference is seen between 1-step MOMF and EHVI. *Right:* The mean hypervolume of 10 trials for the Park functions is shown. Here again considering a convergence to 90% almost an order of magnitude advantage is seen between the 1-step MOMF and EHVI.

The EHVI converged to a hypervolume of 89.4% at a cost of about 7600, whereas the 1-step MOMF reached 90% hypervolume coverage at a cost of about 560. This results in a cost reduction factor of about 13, very similar to the Branin-Currin problem.

It should be noted that the cost reduction is intrinsically linked to the cost ratio between lowest and highest fidelity. In our examples, this ratio was 1:120 and thus, the highest possible cost reduction by taking only lowest fidelity data points would be 120. Averaging the fidelity of the 1-step MOMF over 10 trials and 150 iterations for both Branin-Currin and Park functions yields $\bar{s} \simeq 0.30$ and $\bar{s} \simeq 0.32$, respectively. This results in an average cost of 4.3 and 4.6 per iteration, while the conventional EHVI is fixed to a cost of 120. Thus, a cost reduction of 26 is the maximum that could be achieved if the information gain were the same at all fidelity levels. However, this is generally not the case and low-cost approximations do normally not carry as much information as the highest fidelity. In our case, we see a cost reduction of about half this best possible value, i.e. a cost reduction factor of 13 in both considered test cases. The cost reduction factor can be even higher when the ratio between the cost at highest and the lowest fidelity is increased. For instance, at a maximum cost ratio of 1200:1 for the Branin-Currin problem we measure a cost reduction factor of 44 for convergence to 90% of the hypervolume.

3 Summary and outlook

To conclude, we have demonstrated simultaneous multi-fidelity and multi-objective optimization with a cost reduction of more than an order of magnitude for test problems with a cost ratio of 1:120. The 1-step MOMF also converged to a higher hypervolume when compared with EHVI. An upper limit to the cost reduction factor was also discussed which can be increased by increasing the cost ratio between the highest and lowest fidelity. These results show that MOMF offers significant cost advantage for applications where the goal is to optimize multiple objectives while having access to lower fidelity data.

Our methods build up on existing acquisition functions and can easily be implemented in optimized Bayesian optimization frameworks such as BoTorch (Balandat et al. 2020). This also means that the method can be readily extended e.g. to batch optimization. Code samples for the benchmark cases

have been made available online¹. Since many complex problems in physics and engineering can be simulated with a varying degree of accuracy, our work is crucial in optimizing conflicting objectives in such simulations. This work can also be applied in other areas where optimizing different objectives is advantageous while having access to cheaper evaluations of the functions. The algorithm is flexible in nature since the idea can be applied to any other multi-objective, single-fidelity acquisition function by introducing a fidelity objective and penalizing the acquisition value by the cost. Both methods of MOMF can also be easily extended to include multiple fidelity dimensions, thus allowing efficient optimization over e.g. different resolution parameters in numerical simulations.

Acknowledgements

This work was supported by the DFG through the Cluster of Excellence Munich-Centre for Advanced Photonics (MAP EXC 158), TR-18 funding schemes and the Max Planck Society. It was also supported by the Independent Junior Research Group "Characterization and control of high-intensity laser pulses for particle acceleration", DFG Project No. 453619281. F.I. is part of the Max Planck School of Photonics supported by BMBF, Max Planck Society, and Fraunhofer Society.

¹<https://github.com/PULSE-ML/MOMFBO-Algorithm>

4 Appendix

4.1 Notation

Notation	Description
$\mathbf{x}, \mathbf{y}, \mathbf{f}, s$	bold notation for vectors
f_1, f_2, \dots, f_k	k number of objective functions
\mathbf{x}, \mathbf{y}	input and output vector
\mathbf{f}, s	vector of objective functions and fidelity vector
y_k^s	value of kth function evaluated at fidelity s
λ_k^s	cost of evaluating kth function at fidelity s
\mathcal{Y}^*	true Pareto front at the highest fidelity

4.2 Test functions

In this section we describe the analytical functions used to benchmark the performance of our algorithm. As this is one of the first studies on combined multi-objective and multi-fidelity optimization, we could not directly use test functions from the literature but had to modify them to incorporate an additional fidelity input dimension and exhibit trade-off behavior between the objectives.

4.2.1 Modified multi-fidelity Forrester function

The original Forrester function is

$$f(x) = (6x - 2)^2 \cdot \sin(12x - 4) + 7.025$$

and we use the following modified version as multi-fidelity reference case:

$$f(x, s) = D(s) \cdot [E - g(x, s)]$$

where

$$g(x, s) = A(s) \cdot f[x - 0.2(1 - x \cdot s)] + B(s) \cdot (x - 0.5) - C(s)$$

with $A = 0.5 + 0.5s$, $B = 2 - 2s$, $C = 5s - 5$, $D = 1.5 - 0.5s$ and $E = 25$. The most important differences to other multi-fidelity versions of this function are that it contains a fidelity- and position-dependent shift $\tilde{x}(x, s) = x - 0.2(1 - x \cdot s)$, is inverted for maximization ($E - g(x, s)$ term), the value of the maxima along the fidelity is decreasing ($D(s)$ term) and the maxima are continuously connected from at low to high fidelity.

4.2.2 Modified multi-fidelity, multi-objective Branin-Currin function

Two popular functions used for optimization benchmarking are Branin-Currin functions which were also modified. The usual form of the Branin function is

$$B(\mathbf{x}) = a(x_2 - bx_1^2 + cx_1 - r)^2 + p(1 - t) \cos(x_1) + p,$$

where values of the constants were taken to be $a = 1$, $b = 5.1/(4\pi^2)$, $c = 5/\pi$, $r = 6$, $p = 10$, $t = 1/(8\pi)$ and the form of Currin function is

$$C(\mathbf{x}) = \left[1 - \exp\left(-\frac{1}{2x_2}\right)\right] \frac{2300x_1^3 + 1900x_1^2 + 2092x_1 + 60}{100x_1^3 + 500x_1^2 + 4x_1 + 20}.$$

Both of these functions were modified to make the range of input and output values to be between 0 and 1, i.e. $x_i, y_i \in [0, 1] \forall i = [1, 2]$. The modified form that was used for the Branin is

$$B(\mathbf{x}, s) = -[a(x_{22} - b(s)x_{11}^2 + c(s)x_{11} - r)^2 + p(1 - t(s)) \cos(x_{11}) + p]$$

where $x_{11} = 15(x_1) - 5$, $x_{22} = 15x_2$, $a = 1$, $b(s) = 5.1/(4\pi^2) - 0.01(1 - s)$, $c(s) = 5/\pi - 0.1(1 - s)$, $r = 6$, $p = 10$, $t(s) = (1/(8\pi)) + 0.05(1 - s)$ was used. The x_{11} and x_{22} are used to scale the original domain of the Branin to [0,1]. The main difference is the addition of fidelity

parameter s which for a value of 1 yields the original Branin function and since we are maximizing the problem a minus sign is added. The modified form for the Currin function is

$$C(\mathbf{x}, s) = - \left[\left[1 - (0.1)(1 - s) \exp \left(-\frac{1}{2x_2} \right) \right] \frac{2300x_1^3 + 1900x_1^2 + 2092x_1 + 60}{100x_1^3 + 500x_1^2 + 4x_1 + 20} \right]$$

where again the main difference is the addition of fidelity term $1 - s$ and the addition of a minus sign for maximization.

4.2.3 Modified multi-fidelity multi-objective Park functions

For a benchmark of the multi-objective multi-fidelity problem in higher dimensions, multi-fidelity versions of Park 1 and Park 2 functions were used. The original form of the Park functions is

$$P_1(\mathbf{x}) = \frac{x_1}{2} \left[\sqrt{1 + (x_2 + x_3^2) \frac{x_4}{x_1^2}} - 1 \right] + (x_1 + 3x_4) \exp [1 + \sin(x_3)]$$

$$P_2(\mathbf{x}) = \frac{2}{3} \exp (x_1 + x_2) - x_4 \sin (x_3) + x_3$$

We modified the above two Park functions adding a fidelity dimension (s). To achieve a reasonable Pareto front for optimization, the two functions were also slightly modified. The location of the Pareto set was also modified to not have all the optimizing points in the corners of the 4-D hypercube. A last modification is shifting the Pareto front of the Park functions by subtraction to place a higher importance on the trade-off region. The final form of the two modified Park functions was

$$P_1(\mathbf{x}', s) = A(s) [T_1 + T_2 - B(s)] / 22 - 0.8$$

$$T_1 = \left[\frac{x_1 + 0.001(1 - s)}{2} \right] \cdot \left[\sqrt{1 + (x_2 + x_3^2) \frac{x_4}{x_1^2}} \right]$$

$$T_2 = (x_1 + 3x_4) \exp [1 + \sin(x_3)]$$

$$P_2(\mathbf{x}', s) = A(s) \left[5 - \frac{2}{3} \exp (x_1 + x_2) - (x_4) \sin (x_3) A(s) + x_3 - B(s) \right] / 4 - 0.7$$

where $A(s) = (0.9 + 0.1s)$ and $B(s) = 0.1 * (1 - s)$. Both Park functions now contain a fidelity parameter s . These Park functions are evaluated on a transformed input space

$$[x_1, x_2, x_3, x_4] \rightarrow [1 - 2(x_1 - 0.6)^2, x_2, 1 - 3(x_3 - 0.5)^2, 1 - (x_4 - 0.8)^2].$$

References

- [1] Sergios Theodoridis. *Machine learning: a Bayesian and optimization perspective*. Academic press, 2015.
- [2] Rajesh Kumar Arora. *Optimization: algorithms and applications*. Chapman and Hall/CRC, 2019.
- [3] RJ Shalloo et al. “Automation and control of laser wakefield accelerators using Bayesian optimization”. *Nature communications* 11.1 (2020), pp. 1–8.
- [4] Sören Jalas et al. “Bayesian Optimization of a Laser-Plasma Accelerator”. *Physical review letters* 126.10 (2021), p. 104801.
- [5] Biswajit Paria, Kirthevasan Kandasamy, and Barnabás Póczos. “A flexible framework for multi-objective bayesian optimization using random scalarizations”. *Uncertainty in Artificial Intelligence*. PMLR. 2020, pp. 766–776.
- [6] Kalyanmoy Deb. “Multi-objective optimization”. *Search methodologies*. Springer, 2014, pp. 403–449.
- [7] Jürgen Branke et al. *Multiobjective optimization: Interactive and evolutionary approaches*. Vol. 5252. Springer Science & Business Media, 2008.
- [8] Eckart Zitzler and Lothar Thiele. “Multiobjective evolutionary algorithms: a comparative case study and the strength Pareto approach”. *IEEE transactions on Evolutionary Computation* 3.4 (1999), pp. 257–271.

- [9] Kalyanmoy Deb and J. Sundar. “Reference Point Based Multi-Objective Optimization Using Evolutionary Algorithms”. *Proceedings of the 8th Annual Conference on Genetic and Evolutionary Computation*. GECCO '06. Seattle, Washington, USA: Association for Computing Machinery, 2006, pp. 635–642. ISBN: 1595931864. URL: <https://doi.org/10.1145/1143997.1144112>.
- [10] Joshua Knowles. “ParEGO: A hybrid algorithm with on-line landscape approximation for expensive multiobjective optimization problems”. *IEEE Transactions on Evolutionary Computation* 10.1 (2006), pp. 50–66.
- [11] Wolfgang Ponweiser et al. “Multiobjective optimization on a limited budget of evaluations using model-assisted \mathcal{S} -metric selection”. *International Conference on Parallel Problem Solving from Nature*. Springer. 2008, pp. 784–794.
- [12] Michael Emmerich and Jan-Willem Klinkenberg. “The computation of the expected improvement in dominated hypervolume of Pareto front approximations”. *Rapport technique, Leiden University* 34 (2008), pp. 7–3.
- [13] Daniel G Krige. “A statistical approach to some basic mine valuation problems on the Witwatersrand”. *Journal of the Southern African Institute of Mining and Metallurgy* 52.6 (1951), pp. 119–139.
- [14] Georges Matheron. “Principles of geostatistics”. *Economic geology* 58.8 (1963), pp. 1246–1266.
- [15] Bobak Shahriari et al. “Taking the human out of the loop: A review of Bayesian optimization”. *Proceedings of the IEEE* 104.1 (2015), pp. 148–175.
- [16] Laurence Charles Ward Dixon. “The global optimization problem. an introduction”. *Toward global optimization* 2 (1978), pp. 1–15.
- [17] Carla Currin et al. “Bayesian prediction of deterministic functions, with applications to the design and analysis of computer experiments”. *Journal of the American Statistical Association* 86.416 (1991), pp. 953–963.
- [18] Carl Edward Rasmussen. “Gaussian processes in machine learning”. *Summer school on machine learning*. Springer. 2003, pp. 63–71.
- [19] Jonas Mockus. “Application of Bayesian approach to numerical methods of global and stochastic optimization”. *Journal of Global Optimization* 4.4 (1994), pp. 347–365.
- [20] Peter I Frazier, Warren B Powell, and Savas Dayanik. “A knowledge-gradient policy for sequential information collection”. *SIAM Journal on Control and Optimization* 47.5 (2008), pp. 2410–2439.
- [21] Warren Scott, Peter Frazier, and Warren Powell. “The correlated knowledge gradient for simulation optimization of continuous parameters using gaussian process regression”. *SIAM Journal on Optimization* 21.3 (2011), pp. 996–1026.
- [22] Philipp Hennig and Christian J Schuler. “Entropy Search for Information-Efficient Global Optimization.” *Journal of Machine Learning Research* 13.6 (2012).
- [23] Zi Wang and Stefanie Jegelka. “Max-value entropy search for efficient Bayesian optimization”. *International Conference on Machine Learning*. PMLR. 2017, pp. 3627–3635.
- [24] Dennis D Cox and Susan John. “A statistical method for global optimization”. *[Proceedings] 1992 IEEE International Conference on Systems, Man, and Cybernetics*. IEEE. 1992, pp. 1241–1246.
- [25] Deng Huang et al. “Sequential kriging optimization using multiple-fidelity evaluations”. *Structural and Multidisciplinary Optimization* 32.5 (2006), pp. 369–382.
- [26] Victor Picheny et al. “Quantile-based optimization of noisy computer experiments with tunable precision”. *Technometrics* 55.1 (2013), pp. 2–13.
- [27] Kevin Swersky, Jasper Snoek, and Ryan Prescott Adams. “Multi-task bayesian optimization” (2013).
- [28] Aaron Klein et al. “Fast bayesian optimization of machine learning hyperparameters on large datasets”. *Artificial Intelligence and Statistics*. PMLR. 2017, pp. 528–536.
- [29] Mark McLeod, Michael A Osborne, and Stephen J Roberts. “Practical bayesian optimization for variable cost objectives”. *arXiv preprint arXiv:1703.04335* (2017).
- [30] Yehong Zhang et al. “Information-based multi-fidelity Bayesian optimization”. *NIPS Workshop on Bayesian Optimization*. 2017.

[31] Rémi Lam, Douglas L Allaire, and Karen E Willcox. “Multifidelity optimization using statistical surrogate modeling for non-hierarchical information sources”. *56th AIAA/ASCE/AHS/ASC Structures, Structural Dynamics, and Materials Conference*. 2015, p. 0143.

[32] Shion Takeno et al. “Multi-fidelity Bayesian optimization with max-value entropy search and its parallelization”. *International Conference on Machine Learning*. PMLR. 2020, pp. 9334–9345.

[33] Kirthevasan Kandasamy, Gautam Dasarathy, Barnabas Poczos, et al. “The multi-fidelity multi-armed bandit”. *Advances in neural information processing systems* 29 (2016), pp. 1777–1785.

[34] Kirthevasan Kandasamy, Gautam Dasarathy, Jeff Schneider, et al. “Multi-fidelity bayesian optimisation with continuous approximations”. *International Conference on Machine Learning*. PMLR. 2017, pp. 1799–1808.

[35] Jian Wu and Peter I Frazier. “Continuous-fidelity Bayesian optimization with knowledge gradient” (2018).

[36] Jian Wu, Saul Toscano-Palmerin, et al. “Practical multi-fidelity bayesian optimization for hyperparameter tuning”. *Uncertainty in Artificial Intelligence*. PMLR. 2020, pp. 788–798.

[37] Kaifeng Yang, Michael Emmerich, André Deutz, and Thomas Bäck. “Multi-objective Bayesian global optimization using expected hypervolume improvement gradient”. *Swarm and evolutionary computation* 44 (2019), pp. 945–956.

[38] Michael TM Emmerich, Kyriakos C Giannakoglou, and Boris Naujoks. “Single-and multi-objective evolutionary optimization assisted by Gaussian random field metamodels”. *IEEE Transactions on Evolutionary Computation* 10.4 (2006), pp. 421–439.

[39] Ivo Couckuyt, Dirk Deschrijver, and Tom Dhaene. “Fast calculation of multiobjective probability of improvement and expected improvement criteria for Pareto optimization”. *Journal of Global Optimization* 60.3 (2014), pp. 575–594.

[40] Chang Luo, Koji Shimoyama, and Shigeru Obayashi. “Kriging model based many-objective optimization with efficient calculation of expected hypervolume improvement”. *2014 IEEE Congress on Evolutionary Computation (CEC)*. IEEE. 2014, pp. 1187–1194.

[41] Koji Shimoyama, Shinkyu Jeong, and Shigeru Obayashi. “Kriging-surrogate-based optimization considering expected hypervolume improvement in non-constrained many-objective test problems”. *2013 IEEE Congress on Evolutionary Computation*. IEEE. 2013, pp. 658–665.

[42] Michael TM Emmerich, André H Deutz, and Jan Willem Klinkenberg. “Hypervolume-based expected improvement: Monotonicity properties and exact computation”. *2011 IEEE Congress of Evolutionary Computation (CEC)*. IEEE. 2011, pp. 2147–2154.

[43] Iris Hupkens et al. “Faster exact algorithms for computing expected hypervolume improvement”. *international conference on evolutionary multi-criterion optimization*. Springer. 2015, pp. 65–79.

[44] Michael Emmerich, Kaifeng Yang, et al. “A multicriteria generalization of bayesian global optimization”. *Advances in Stochastic and Deterministic Global Optimization*. Springer, 2016, pp. 229–242.

[45] Kaifeng Yang, Michael Emmerich, André Deutz, and Carlos M Fonseca. “Computing 3-D expected hypervolume improvement and related integrals in asymptotically optimal time”. *International Conference on Evolutionary Multi-Criterion Optimization*. Springer. 2017, pp. 685–700.

[46] Samuel Daulton, Maximilian Balandat, and Eytan Bakshy. “Differentiable expected hypervolume improvement for parallel multi-objective Bayesian optimization”. *arXiv preprint arXiv:2006.05078* (2020).

[47] Syrine Belakaria, Aryan Deshwal, and Janardhan Rao Doppa. “Multi-fidelity multi-objective bayesian optimization: an output space entropy search approach”. *Proceedings of the AAAI Conference on artificial intelligence*. Vol. 34. 06. 2020, pp. 10035–10043.

[48] Maximilian Balandat et al. “BoTorch: A framework for efficient Monte-Carlo Bayesian optimization”. *Advances in Neural Information Processing Systems (NeurIPS)* (2020).

[49] Jeong Soo Park. “Tuning complex computer codes to data and optimal designs”. PhD thesis. University of Illinois at Urbana-Champaign, 1991.